J|A|C|S COMMUNICATIONS

Published on Web 04/14/2010

Direct Use of ^{15}N Relaxation Rates as Experimental Restraints on Molecular Shape and Orientation for Docking of Protein−Protein Complexes

Yaroslav Ryabov,[†] G. Marius Clore,*[,‡] and Charles D. Schwieters*[,†]

Division of Computational Bioscience, Building 12A, Center for Information Technology, National Institutes of Health, Bethesda, Maryland 20892-5624, and, Laboratory of Chemical Physics, Building 5, National Institutes of Diabetes and Digestive and Kidney Diseases, National Institutes of Health, Bethesda, Maryland 20892-0520

Received March 4, 2010; E-mail: mariusc@mail.nih.gov; charles.schwieters@nih.gov

Protein−protein interactions play a central role in a multitude of biological processes. While full structure determination of protein−protein complexes by crystallography or NMR spectroscopy is clearly desirable, it may not always be possible. In the case of NMR spectroscopy, it is also the case that the larger the system, the more difficult it is to acquire and analyze intermolecular nuclear Overhauser enhancement data to derive interproton distance restraints that are the mainstay of conventional NMR structure determination.[1] While technical improvements have been made in *ab initio* protein docking, it is still not particularly reliable.[2] For this reason, recent efforts have been focused on developing methods that can make use of sparse solution experimental data.[3,4] For example, incorporation of highly ambiguous distance restraints derived from chemical shift perturbation mapping can facilitate protein docking,[3,4] and reliability can be further improved by the addition of orientational restraints derived from residual dipolar couplings (RDCs).[4]

Supplementary structural information also resides in ^{15}N transverse (R_2) and longitudinal (R_1) relaxation rates. In the absence of large scale internal motions or conformational exchange line broadening, ^{15}N R_2/R_1 ratios depend on only two factors: the rotational diffusion tensor which is related to the size and shape of the complex[5] and the orientation of N−H bond vectors relative to the axes of the diffusion tensor.[5−8] In initial work,[8] ^{15}N R_2/R_1 ratios were employed in a manner analogous to RDCs[9] to provide N−H bond orientational restraints with predetermined, approximate values of the magnitude of the diffusion tensor estimated directly from the distribution of measured R_2/R_1 ratios.[10] Recently, fast methods for computing the rotational diffusion tensor based on molecular structure[11] have permitted direct refinement against the components of the rotational diffusion tensor,[12] thereby incorporating information on molecular shape and size from relaxation measurements that is not dissimilar to that afforded by solution small-angle X-ray scattering. Here we describe a new approach in which ^{15}N R_2/R_1 relaxation data are used to simultaneously provide information on both molecular shape and N−H bond orientations without requiring prior information to be extracted from either the data or a known molecular structure. The application to protein−protein docking by conjoined rigid body/torsion angle simulated annealing[13] is illustrated using the complex of the N-terminal domain of enzyme I (EIN) and HPr,[12,14] and the HIV-1 protease dimer[7,15] as examples.

Conceptually, the elements of the rotational diffusion tensor are calculated from the atomic coordinates at each step of the simulated annealing protocol and then used together with the N−H bond vector orientations to compute the ^{15}N R_2/R_1 ratios. The pseudopotential energy term, E_{relax}, that is minimized in the Xplor-NIH (v2.25) structure determination package[16] is given by

$$E_{relax} = k_{relax} \sum_{i=1}^{N} (\rho_i^{calc} - \rho_i^{obs})^2/\sigma_i^2 \qquad (1)$$

where ρ_i^{calc} and ρ_i^{obs} are the calculated and observed R_2/R_1 ratios, respectively, for residue i; σ_i is the corresponding experimental error in the measurements; N is the number of data points; and k_{relax} is a force constant. ρ_i^{calc} is obtained from the spectral density function, $J_i(\omega)$ (ignoring the very small contribution from ^{15}N chemical shift anisotropy):[17]

$$\rho_i^{calc} = \frac{4J_i(0) + 6J_i(\omega_H - \omega_N) + J_i(\omega_H + \omega_N) + 6J_i(\omega_H) + 3J_i(\omega_N)}{2[6J_i(\omega_H - \omega_N) + J_i(\omega_H + \omega_N) + 3J_i(\omega_N)]} \qquad (2)$$

where ω_H and ω_N are the ^{1}H and ^{15}N nuclear Lamor frequencies. $J_i(\omega)$ is expressed as

$$J_i(\omega) = \frac{2}{5} \sum_{r=-2}^{2} \frac{E_r}{E_r^2 + \omega^2} F_r(\{D_x, D_y, D_z\}, \Omega_{D \to A_i}) \qquad (3)$$

where the values of E_r are frequencies depending on the three eigenvalues, D_x, D_y, and D_z, of the rotational diffusion tensor **D**; and the function F_r depends on the same set of eigenvalues and on the orientation of the N−H bond of residue A_i relative to the principal axis of **D** (see Supporting Information for details). **D** is calculated from the atomic coordinates by representing the surface of the protein by an equivalent ellipsoid and then applying Perrin's equations[18] to calculate **D** from the dimensions and orientation of the ellipsoid.[12] The gradients of E_{relax} with respect to all atomic displacements are evaluated in closed form and used to calculate the atomic forces during gradient minimization and molecular dynamics. In addition to molecular size and shape, **D** also depends on the solvent viscosity and temperature. To account for uncertainties in the latter, the apparent diffusion tensor temperature (which is not a physical temperature but a fitting parameter) is also optimized during minimization and simulated annealing.[12]

In the context of docking, highly ambiguous distance restraints (E_{CSMap}) derived from chemical shift perturbation mapping serve to delineate the interaction surface,[3,4] while the incorporation of the E_{relax} potential provides simultaneous restraints on the molecular shape and size of the complex and on the relative orientation of the proteins within the complex. The other terms included in the target function are covalent geometry terms, a knowledge-based low-resolution hydrophobic contact potential,[12] a multidimensional torsion angle database potential of mean force,[19] and a quartic van der Waals repulsion term (E_{repel}).[20] Briefly, the protocol consists of initial rigid body minimization starting from randomized positions

[†] Center for Information Technology.
[‡] National Institutes of Diabetes and Digestive and Kidney Diseases.

and orientations of the two proteins subject to only E_{CSMap}, E_{relax}, and E_{repel} (applied to only the Cα atoms at this initial stage). This is followed by conjoined rigid body/torsion angle dynamics simulated annealing in which the backbone and internal side chains of each protein are treated as rigid bodies with translational and rotational degrees of freedom and the surface side chains are given full torsional degrees of freedom. The force constants for the various terms in the target function are progressively ramped up as the temperature is decreased from 1000 to 10 K. A full description is provided in Supporting Information.

The ^{15}N R_2/R_1 ratios are subject to uncertainties arising from both errors in the protein backbone coordinates (that are treated as rigid bodies) and the presence of significant local motions (either on the sub-nanosecond or μs-ms time scales which decrease and increase the R_2/R_1 ratios, respectively). Since EIN and hence the EIN−HPr complex are highly anisotropic,[8] anomalous ^{15}N R_2/R_1 data were identified in an iterative fashion; the experimental R_2/R_1 data[12] were fit to the X-ray coordinates of free EIN[21] and HPr[22] separately by optimizing the respective diffusion tensors (while restraining the anisotropy and rhombicity to be the same) and excluding from further analysis data for those residues with relative deviations larger than 1.5σ between observed and calculated ^{15}N R_2/R_1 ratios (this corresponds to excluding 13% of the data; see Supporting Information). The starting coordinates were the X-ray structures of free EIN[21] and HPr[22] with the torsion angles of the surface side chains partially randomized (by a 1 ns run of torsion angle dynamics at 3000 K with the backbone fixed). The reference structure was generated by best-fitting the backbone of the X-ray coordinates of the free structures onto the NMR structure of the complex,[14] so that the calculated atomic rms differences reflect only differences in the positions of the two proteins relative to one another in the complex. A total of 512 structures were calculated.

Figure 1 compares the dependence of the total energy on the Cα rms difference between the calculated structures, without (Figure 1A and B) and with (Figure 1C and D) the inclusion of the E_{relax} potential, and the minimum energy (left panels) or reference (right panels) structure. Cluster analysis relative to the respective minimum energy structures[12] shows that 40% of the structures lie within the cluster containing the minimum energy structure when both E_{CSMap} and E_{relax} potentials are used compared to 36% when E_{CSMap} alone is used. The inclusion of E_{relax}, however, results in better discrimination (cf. compare Figure 1A with Figure 1C, and Figure 1B with Figure 1D): the 10 lowest energy structures have a backbone accuracy of ~1.6 Å, and the data clearly show that the introduction of E_{relax} results in an approximately 2-fold improvement in both backbone accuracy and precision, compared to structures calculated with only the E_{CSMap} term (Table 1).

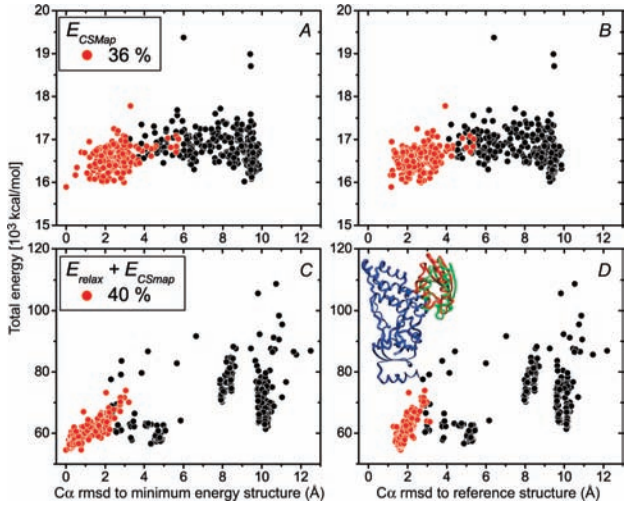

Figure 1. Docking of the EIN−HPr complex using ^{15}N R_2/R_1 relaxation data. Dependence of the total energy on the Cα rms difference from the minimum energy docked structures (left panels) and the reference structure (right panels) for calculations based on E_{CSMap} alone (A and B) and in combination with E_{relax} (C and D). Structures located in the cluster that includes the minimum energy structure are indicated by the red filled-in circles. The inset in the lower right-panel shows a comparison of the location of HPr in the restrained regularized mean docked structure derived from the lowest 10 energy structures calculated using both E_{CSMap} and E_{relax} (red) with the position of HPr in the reference structure (green); the backbone of EIN is shown in blue. T_{diff}^{app} was optimized independently for EIN and HPr within a range of 313 ± 10 K, and the nominal experimental temperature was 313 K.

Table 1. Impact of E_{relax} on Docking Accuracy of the EIN/HPr Complex

	E_{CSMap}	$E_{relax} + E_{CSMap}$
Precision (Å)[a]	1.8 ± 2.7	0.3 ± 0.2
Accuracy (Å)[b]	3.2 ± 2.3	1.6 ± 0.1
Mean coordinate accuracy (Å)[c]	2.4	1.6
$\langle(\rho_i^{calc} - \rho_i^{obs})^2\rangle^{1/2}$ [d]	2.51 ± 0.17	2.29 ± 0.01

[a] Cα rmsd from the mean coordinates averaged over the 10 lowest energy structures. [b] Cα rmsd from reference coordinates averaged over the 10 lowest energy structures. [c] Cα rmsd between restrained regularized mean and reference structure. [d] This is the rms deviation averaged over all R_2/R_1 experimental data. The value for the reference structure is 2.4, and the values of ρ_i span from ~20 to ~40.

We also carried out calculations using only the E_{relax} term in the absence of the E_{CSMap} restraints. For the EIN/HPr complex docking with only the E_{relax} term generated several clusters of solutions due to degeneracy in the orientations of the principal axis frame of the diffusion tensors (Figure 2). Three of the clusters (denoted as A, B, and C and comprising 5, 16, and 1% of the calculated structures, respectively) have approximately the same minimum energy which, most probably, reflects the fact that for those clusters the nearly spherical shape of HPr does not provide sufficient differentiation between the alternate HPr orientations and locations that satisfy the orientational restraints from the E_{relax} term. However, the clusters

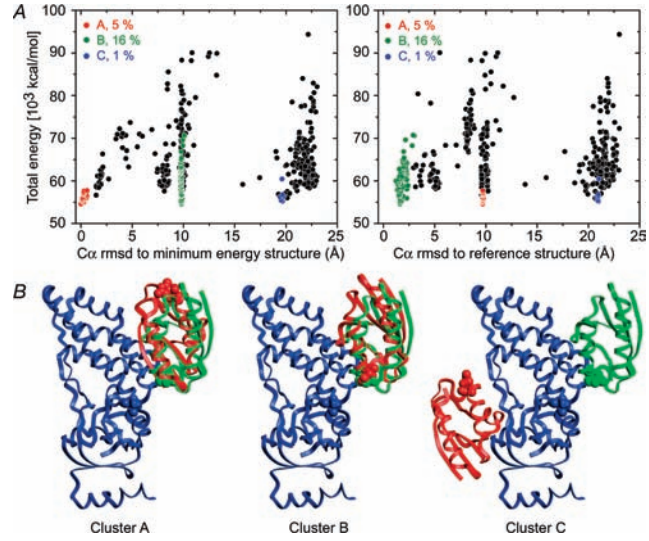

Figure 2. Docking of the EIN/HPr complex based only on the E_{relax} potential for the ^{15}N R_2/R_1 relaxation data. (A) Dependence of the total energy on the Cα rms difference from the minimum energy docked structure (left panel) and the reference structure (right panel). There are three main clusters, A, B, and C, denoted by red, green, and blue circles. (B) Comparison of the location of HPr in the restrained regularized mean docked EIN/HPr complexes (red) with that in the reference structure (green). The backbone of EIN is shown in blue; the active site histidines are depicted as space-filling models in the same color as the corresponding backbone.

Table 2. Docking of the EIN/HPr Complex Using Only E_{relax}

	Cluster A	Cluster B	Cluster C
Precision (Å)[a]	0.16 ± 0.07	0.40 ± 0.27	0.33 ± 0.15
Accuracy (Å)[a]	9.67 ± 0.02	1.73 ± 0.20	20.93 ± 0.08
Mean coordinate accuracy (Å)[a]	9.70	1.68	20.94
$\langle(\rho_i^{calc} - \rho_i^{obs})^2\rangle^{1/2}$	2.32 ± 0.01	2.29 ± 0.01	2.27 ± 0.01
CSMap distance violations (Å)[b]	10.8 ± 0.4	0.0 ± 0.0	29.0 ± 0.0
Cα−Cα distance between active site histidines (Å)[c]	35.7 ± 0.2	15.1 ± 0.5	29.9 ± 0.5
RDC R-factor (%)[d]	37.0 ± 0.2	30.1 ± 1.0	36.2 ± 0.7

[a] As defined in Table 1, footnotes a−c. [b] Violations of >0.5 Å for the highly ambiguous distance restraints derived from chemical shift perturbation mapping. [c] The active site histidines are His-189 of EIN and His-15 of HPr. [d] The RDC *R*-factor obtained by singular value decomposition is given by $\{\langle D_{obs} - D_{calc})^2\rangle/(2\langle D_{obs}{}^2\rangle)\}^{1/2}$, where D_{obs} and D_{calc} are the observed and calculated RDCs, respectively.[23] The RDC *R*-factor for the reference structure is 27%.

can readily be differentiated and the correct solution ascertained by rescoring the results based on the number of E_{CSMap} distance violations or using other experimental information (Table 2). For example, in the case of the EIN/HPr complex, the distance between the Cα atoms of His-189 of EIN and His-15 of HPr must be within 11−16 Å to permit phosphoryl transfer to occur between EIN and HPr.[14] On the basis of either criterion, cluster B, which is ∼1.7 Å from the reference structure, can be unambiguously identified as the correct solution. This is further confirmed by validation against backbone amide RDCs[14] which provide independent orientational information.

Inclusion of RDCs in the docking calculations may increase discrimination and convergence by reducing orientational degeneracy.[4,9] Thus when E_{relax} is supplemented by an RDC potential term[16] for backbone amide RDCs (measured in a charged liquid crystalline medium),[14] but omitting the E_{CSMap} term, the cluster containing the minimum energy structure is clearly distinct from other clusters and corresponds to the correct solution with a mean coordinate accuracy of 1.5 Å for the 10 lowest energy structures.

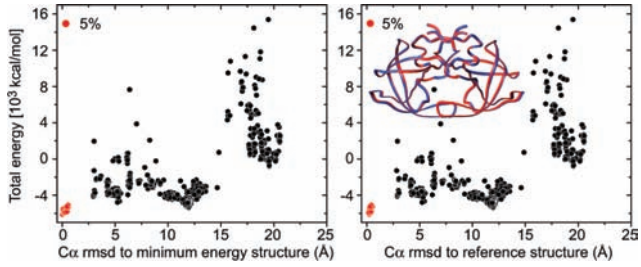

Figure 3. Docking of the symmetric HIV-1 protease dimer using the E_{relax} potential for the ^{15}N R_2/R_1 relaxation data. Dependence of the total energy on the Cα rms difference from the minimum energy docked structure (left) and the symmetrized reference X-ray structure[15] (right). Structures located in the cluster that includes the minimum energy structure, are indicated by the red filled-in circles and comprise 5% of the total number of calculated structures. The precision and accuracy of the 10 lowest energy structures are 0.14 ± 0.05 and 0.30 ± 0.06 Å, respectively; the mean coordinate accuracy is 0.31 Å; and the rms difference between observed and calculated ^{15}N R_2/R_1 ratios is 0.35 (compared to 0.48 for the reference X-ray structure). The inset in the right panel shows a backbone superposition (displayed as tubes) of the restrained regularized mean docked structure (red) and the crystal structure (blue). T_{diff}^{app} was optimized within the range 300 ± 5 K, and the nominal experimental temperature was 300 K.

Similar docking calculations were also carried out for the symmetric HIV-1 protease dimer[7,15] using the E_{relax} potential but, in addition, included two symmetry restraints, one to confer C_2 symmetry and the other to ensure that the coordinates of the surface side chains remain identical for both subunits.[12] The 10 lowest energy structures converge to the correct solution with a backbone coordinate accuracy of ∼0.3 Å relative to the X-ray coordinates[15] (Figure 3).

In conclusion, we have shown that the shape and orientational information afforded by directly using ^{15}N R_2/R_1 relaxation data in structure calculations without the need for any prior assumptions, combined with minimal additional information in the form of highly ambiguous distance restraints derived from chemical shift perturbation mapping, additional biochemical data, or, in the case of dimers, symmetry restraints, provides a powerful tool to facilitate reliable docking of protein−protein complexes.

Acknowledgment. Y.R. acknowledges a National Research Council Research Associateship. This work was supported by the NIH Intramural Research Programs of NIDDK (G.M.C.) and CIT (C.D.S.).

Supporting Information Available: Details of the algorithm, docking protocol, data treatment, Xplor-NIH scripts, and experimental restraints files. This material is available free of charge via the Internet at http://pubs.acs.org.

References

(1) (a) O'Connell, M. R.; Gamsjaeger, R.; Mackay, J. P. *Proteomics* **2009**, *9*, 5224–5232. (b) Clore, G. M.; Gronenborn, A. M. *Trends Biotechnol.* **1998**, *16*, 22–34.
(2) (a) Lensink, M. F.; Méndez, R.; Wodak, S. J. *Proteins* **2007**, *69*, 704–718. (b) Jajda, S.; Kozakov, D. *Curr. Opin. Struct. Biol.* **2009**, *19*, 164–170.
(3) (a) Dominguez, C.; Boelens, R.; Bonvin, A. J. M. M. *J. Am. Chem. Soc.* **2003**, *125*, 1731–1737. (b) de Vries, S. J.; van Dijk, A. D.; Krzeminski, M.; van Dijk, M.; Thureau, A.; Hsu, V.; Wassenaar, T.; Bonvin, A. M. M. M. *Proteins* **2007**, *69*, 726–733.
(4) Clore, G. M.; Schwieters, C. D. *J. Am. Chem. Soc.* **2003**, *15*, 2902–2912.
(5) Woessner, D. E. *J. Chem. Phys.* **1962**, *37*, 647–654.
(6) Lipari, G.; Szabo, A. *J. Am. Chem. Soc.* **1982**, *104*, 4546–4559.
(7) Tjandra, N.; Wingfield, P. T.; Stahl, S. J.; Bax, A. *J. Biomol. NMR* **1996**, *8*, 273–284.
(8) Tjnadra, N.; Garrett, D. S.; Gronenborn, A. M.; Bax, A.; Clore, G. M. *Nat. Struct. Biol.* **1997**, *4*, 443–449.
(9) Bax, A.; Kontaxis, G.; Tjandra, N. *Methods Enzymol.* **2001**, *339*, 127–174.
(10) Clore, G. M.; Gronenborn, A. M.; Szabo, A.; Tjandra, N. *J. Am. Chem. Soc.* **1998**, *120*, 4889–4890.
(11) Ryabov, Y.; Geraghty, C.; Warshney, A.; Fushman, D. *J. Am. Chem. Soc.* **2006**, *128*, 15432–15444.
(12) Ryabov, Y.; Suh, J.-Y.; Grishaev, A.; Clore, G. M.; Schwieters, C. D. *J. Am. Chem. Soc.* **2009**, *131*, 9522–9531.
(13) Schwieters, C. D.; Clore, G. M. *J. Magn. Reson.* **2001**, *152*, 288–302.
(14) Garrett, D. S.; Seok, Y.-J.; Peterkofsky, A.; Gronenborn, A. M.; Clore, G. M. *Nat. Struct. Biol.* **1999**, *6*, 166–173.
(15) Das, A.; Prashar, V.; Mahale, S.; Serre, L.; Ferrer, J. L.; Hosur, M. V. *Proc. Natl. Acad. Sci. U.S.A.* **2006**, *103*, 18464–18469.
(16) Schwieters, C. D.; Kuszewski, J.; Clore, G. M. *Progr. NMR Spectrosc.* **2006**, *48*, 47–62.
(17) Abragam, A. *The Principles of Nuclear Magnetism*; Clarendon Press: Oxford, 1961.
(18) Perrin, F. J. *Phys. Radium* **1934**, *5*, 497–511.
(19) Clore, G. M.; Kuszewski, J. *J. Am. Chem. Soc.* **2004**, *126*, 7281–7292.
(20) Nilges, M.; Gronenborn, A. M.; Brünger, A. T.; Clore, G. M. *Protein Eng.* **1988**, *2*, 27–38.
(21) Liao, D. I.; Silverton, E.; Seok, Y. J.; Lee, B. R.; Peterkovsky, A.; Davies, D. R. *Structure* **1996**, *4*, 861–872.
(22) Jia, Z. C.; Quail, J. W.; Waygood, E. B.; Delbaere, L. T. J. *J. Biol. Chem.* **1993**, *268*, 22490–22501.
(23) Clore, G. M.; Garrett, D. S. *J. Am. Chem. Soc.* **1999**, *121*, 9008–9012.

JA101842N